IEEE Access
Multidisciplinary | Rapid Review | Open Access Journal

Received July 13, 2021, accepted July 24, 2021, date of publication August 3, 2021, date of current version August 11, 2021.

Digital Object Identifier 10.1109/ACCESS.2021.3102102

Analysis and Small Signal Modeling of Five-Level Series Resonant Inverter

ALLA EDDINE TOUBAL MAAMAR[1], (Graduate Student Member, IEEE), M'HAMED HELAIMI[1], RACHID TALEB[1], MOSTEFA KERMADI[2], (Member, IEEE), SAAD MEKHILEF[2,3,4], (Senior Member, IEEE), ADDY WAHYUDIE[5,6], (Member, IEEE), AND MUHYADDIN RAWA[4], (Member, IEEE)

[1]Laboratoire Génie Electrique et Energies Renouvelables (LGEER), Department of Electrical Engineering, Hassiba Benbouali University of Chlef, Chlef 02180, Algeria
[2]Power Electronics and Renewable Energy Research Laboratory (PEARL), Department of Electrical Engineering, University of Malaya, Kuala Lumpur 50603, Malaysia
[3]School of Science, Computing and Engineering Technologies, Swinburne University of Technology, Melbourne, VIC 3000, Australia
[4]Center of Research Excellence in Renewable Energy and Power Systems, King Abdulaziz University, Jeddah 21589, Saudi Arabia
[5]Department of Electrical Engineering, United Arab Emirates University, Al Ain, United Arab Emirates
[6]National Water and Energy Center (NWEC), UAE-U, Al Ain, United Arab Emirates

Corresponding author: Saad Mekhilef (smekhilef@swin.edu.au)

This work was supported in part by the Asian University Alliance (AUA)–UAE-U under Project 12R022; in part by the Ministry of Higher Education, Malaysia, through the Large Research Grant Scheme (LRGS) under Grant LRGS/1/2019/UKM/01/6/3, and in part by Hassiba Benbouali University of Chlef, Algeria.

ABSTRACT This paper explains the implementation of a small-signal model for a new five-level series resonant inverter structure. The proposed circuit combines the advantages of multilevel inverters and the characteristics of the physical phenomena, resonance. The small-signal model offers the possibility to design a linearized linear time-invariant (LTI) model around an equilibrium point based on the first-order Taylor series. After that, the performance of the proposed five-level series resonant inverter and its small-signal model are evaluated in MATLAB/Simulink environment. Compared with a MATLAB model generated using the system identification toolbox, the developed small-signal model exhibited a good accuracy in frequency and time domains. In addition, a hardware test bench is developed to validate the proposed model. Both simulation and experimental results show that the proposed multilevel resonant inverter is very interesting for high-voltage high-frequency applications. As a perspective, from the results obtained, we suggest the use of small-signal AC analysis for multilevel series resonant inverter modeling. The paper contains rich information on the recently used tools for dynamic systems modeling and analysis of nonlinear processes that can be applied to modeling and analyzing other power electronics inverters.

INDEX TERMS AC analysis of dynamic nonlinear system, five-level series resonant inverter, inverter mathematical model, multilevel inverter simulation, model of inverter, small-signal modeling.

I. INTRODUCTION

In the power electronics domain, there are particular types of inverters known as resonant inverters. These types are used in many power applications, where the generated output voltage of resonant inverter topologies has a high-frequency value [1]. The resonant inverter has received much attention in power electronics research and introduced in a wide range of industry applications, including: power conversion systems [2], induction heating [3], telecommunication and wireless power transfer [4], and ozone generators [5]. The three main structures for realizing a resonant inverter are shown in Fig. 1, namely: series resonant tank, parallel resonant tank, and series-parallel resonant tank [6]. Half-bridge and Full-bridge are the conventional-used topologies for realizing resonant converters [2]. Furthermore, the multilevel inverter is not famous for high-frequency resonant inverters because their modeling for control design is a challenging step, especially the control with high-frequency modulation techniques.

Notwithstanding, emerging single-phase multilevel inverters (MLIs) play a significant role in developing power generation systems. Emerging MLIs topologies have been proposed to overcome the conventional inverters' problems and achieve high efficiency with high power quality [7]–[9]. Recently

The associate editor coordinating the review of this manuscript and approving it for publication was Siqi Bu.

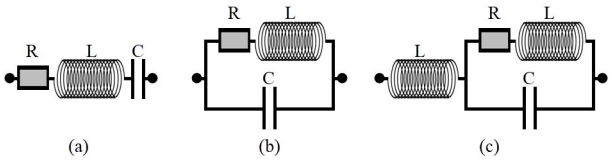

FIGURE 1. Equivalent model of resonant configurations: (a) series, (b) parallel, and (c) hybrid series-parallel.

decade, many hybrid topologies of the converter are discussed to produce a balanced and unbalanced system with self-voltage balancing, such as the fewer number of switches [10], the quadruple boost inverter [11], and dual input switched-capacitor SC-MLI [12]. Thanks to the development of digital control using super calculators, DSP, and embedded boards, the fundamental-switching modulation techniques provide their efficiency in many applications [13]. The fundamental modulation switching can be an excellent solution to open the door for using multilevel inverters in high-frequency, high-power applications. Suppose a use of multilevel topology in resonant inverters for high-frequency applications. In that case, the multilevel inverter can improve the power, and total standing voltage (TSV) in conventional resonant inverters can be resolved [8].

On the other hand, analysis and modeling of the inverter is an essential part of performance tests, and it is the basis for the controller design. The general average model, the average generator model, the average state model method, and small-signal modeling are the most used modeling methods in dynamic system analysis [14], [15]. Various small-signal methods have been proposed. A small-signal model of PWM dc-dc power converters is discussed in [16]. A small-signal modeling of coupled-inductor double-boost converter is presented in [17]. A linearized small-signal model around an equilibrium point of grid-forming modular multi-level converter (MMC) is presented in [18], where the MMC is under the outer voltage control loop and inner current control loop. Small-signal modeling of the thermoelectric generator is discussed in [19], where the model is developed based on physical lows by applying an existing model to the dynamic mode. The model of the thermoelectric generator can be extended for more configurations. A dynamic average model of a grid-connected converter is discussed in [20]. Also, small-signal Ac analysis is used for modeling of unidirectional T-Rectifier as explained in [21]. Furthermore, a new small-signal modeling method was proposed for DC-DC converters in [22]. It is clear from the above-presented studies that modeling of a dynamic system is attracting a lot of researchers, where the purpose is presenting the linear time-invariant (LTI) model beginning from the nonlinear dynamic model.

The conventional modeling technique as the switching model contains complex behavior in the time domain. So, these methods are not able to give the dynamic behavior of the converter. Circuit averaging is a widely known strategy for converter modeling. The averaging approach provides a more physical interpretation of the system model. The average and large signal techniques are nonlinear models. Therefore, they cannot be used to synthesize a continuous or a sampled linear regulator of the studied system. In this context, it is necessary to linearize the model that is also called a tangent model. Two well-known methods exist to linearize a nonlinear dynamic system, linearization around a trajectory and linearization around an equilibrium point. These models make it possible to get rid of nonlinearity problems. The construction of such models requires a Taylor series development limited to the first order. The resulting model is linear, invariant in time, and regulates the inverter's dynamic behavior in a small variation regime around its equilibrium point. The small-signal model offers the possibility to design various linear control methods [23].

In the literature, there are many tools for validating the small-signal modeling of any nonlinear dynamic system, among them: PLECS with AC SWAP, SIMPLIS AC analysis, LTspice AC analysis, MATLAB STREAM in Linearization manager tool. Using the Linearization manager tool with sinestream as the perturbation signal and system identification toolbox is very interesting, as described in [24].

Despite the numerous presented works using Half-bridge and Full-bridge topology in resonant inverters, none of the previous works attempted to use six-switch five-level topology to realize series resonant inverter and model the circuit using small-signal AC analysis. Also, there is a gap in knowledge about applying a small signal method for modeling multilevel power converters [25], where accuracy in mathematical analysis and step-by-step understanding of problem-solving algorithms are needed. Furthermore, it isn't easy to design a classical or advanced controller for nonlinear switching converters using the Simulink SimPower model, where the analysis of dynamic behavior of such nonlinear systems is very complex.

The present work proposes a small-signal model of a five-level series resonant inverter. This study is included in the class of the linearization of a nonlinear dynamic system around an equilibrium point. We follow the existing equivalent circuit model based on fundamental approximation presented in [26] because this analysis works well for series resonant converters [27]. The frequency response of the proposed five-level series resonant inverter model and the frequency response of the developed small-signal model are presented and compared using Matlab tools to validate the proposed small-signal model. This study has the following merits: (1) a new circuit of multi-level resonant inverters is proposed, where the half-bridge and full-bridge are the conventional-used topologies to construct this special type of inverters; (2) the proposed system uses six switches and six gate drivers to produce a high-frequency five-level output voltage; (3) a step-by-step tutorial for modeling the proposed five-level series resonant inverter is presented using small-signal AC analysis. This manuscript will reinforce the information contained in the previous works and give a new perspective about the application of the small-signal method. This paper is

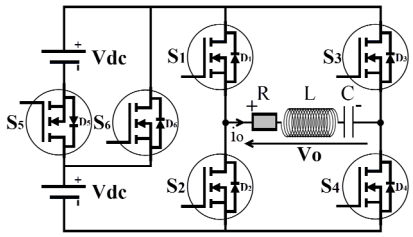

FIGURE 2. The 5-level series resonant inverter structure.

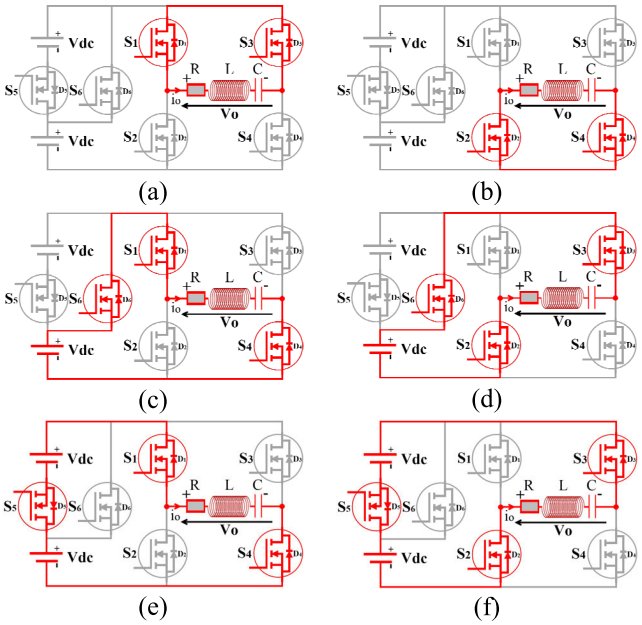

FIGURE 3. Equivalent circuit to produce (a): $V_o = 0$. (b): $V_o = 0$. (c): $V_o = +V_{dc}$. (d): $V_o = -V_{dc}$. (e): $V_o = +2V_{dc}$. (f): $V_o = -2V_{dc}$.

organized as follows: in the section II, the proposed circuit of the five-level inverter operation is presented. The small-signal modeling is discussed in section III. Simulation and experimental results are discussed in section IV, and conclusions are presented in section V.

II. FIVE-LEVEL SERIES RESONANT INVERTER OPERATING PRINCIPLE

The complete configuration of the 5-level series resonant inverter is presented in Fig. 2; the circuit consists of two direct current DC sources, six Mosfets switches, and a series RLC circuit composed of resistor (R), inductance (L), and capacitance (C), respectively.

Summing $V_{dc1} = V_{dc2} = Vdc$ condition, the five-level inverter can produce five output voltage (V_o) levels: $+V_{dc}$, $+2V_{dc}$, 0, $-V_{dc}$, and $-2V_{dc}$ as shown in equivalent circuits presented in Fig. 3. In a complete switching period (T), there are a total of 12 switching transitions of the 5-level inverter. The operation of the switches is periodic and in complementary mode (S_1, S_2), (S_3, S_4) and (S_5, S_6), so we can set (S_a, S_b, S_c) = (S_1, S_3, S_5) to propose the following

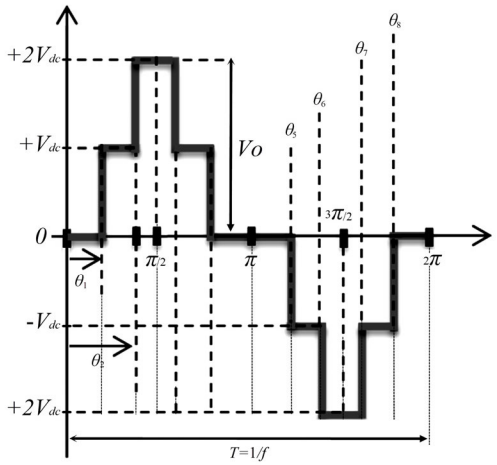

FIGURE 4. The output phase voltage of the five-level inverter.

switching system (1).

$$V_o = \begin{cases} +2Vdc \xrightarrow{if} (S_a, S_b, S_c) = (1, 0, 1) \\ +Vdc \xrightarrow{if} (S_a, S_b, S_c) = (1, 0, 0) \\ 0 \xrightarrow{if} (S_a, S_b) = (0, 0) \; or \; (1, 1) \\ -Vdc \xrightarrow{if} (S_a, S_b, S_c) = (0, 1, 1) \\ -2Vdc \xrightarrow{if} (S_a, S_b, S_c) = (0, 1, 0) \end{cases} \quad (1)$$

III. SMALL-SIGNAL MODELING OF THE FIVE-LEVEL SERIES RESONANT INVERTER

A small-signal model was constructed using the mathematical (analytical) method and validated with simulation tests using Matlab software environments. Small-signal model of the proposed Five-level series resonant inverter based on the following steps:

A. MATHEMATICAL ANALYSIS OF THE FIVE-LEVEL INVERTER OUTPUT VOLTAGE USING FOURIER TRANSFORMATION

Fig. 4 shows the desired output five-level voltage. The inverter's output voltage $V_o(t)$ depends on the time; it can be regulated by modulating the switching frequency ω_s or controlling the switching angles, θ_1 and/or θ_2 or controlling the amplitude V by variation of V_{dc}. Conclude that the operating point is determined by (V, ω_s, θ_1, θ_2). The voltage $V_o(t)$ can be expressed using the Fourier transformation because the signal is even periodic and continue by parts with the following expression:

$$V_o(t) = a_0 + \sum_{n=1}^{\infty} a_n \cos(n\omega_s t) + \sum_{n=1}^{\infty} b_n \sin(n\omega_s t) \quad (2)$$

where, the Fourier parameters can be written as:

$$a_0 = 0, \quad a_n = 0, \; b_n = \frac{2}{T}\int_0^T V(t)\sin(n\omega_s t)dt \quad (3)$$

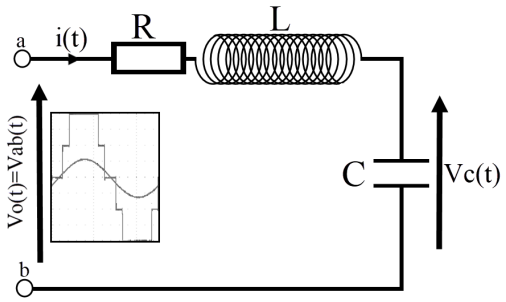

FIGURE 5. The simplified equivalent circuit of the resonant inverter.

The mentioned voltage $V_o(t)$ in expression (2) is calculated using the parameters (3), calculation outcome can be written as:

$$V_o(t) = \sum_{n=1}^{\infty} \left(\frac{4V}{n\pi} \left(\cos(n\theta_1) + \cos(n\theta_2) \right) \right) \sin(n\omega_s t) \quad (4)$$

For $(n = 1)$, the fundamental voltage (also known as the first harmonic) of the voltage $V_o(t)$ can be created as:

$$V_o(t) = \frac{4V}{\pi} \left(\cos(\theta_1) + \cos(\theta_2) \right) \sin(\omega_s t) \quad (5)$$

B. THE EXACT NONLINEAR MODEL OF THE RESONANT INVERTER

The circuit of Fig. 2 is reduced to a simplified form, as shown in Fig. 5. Kirchhoff's laws are applied to the simplified equivalent circuit to give the nonlinear system (6), where $i(t)$ is the current.

$$\begin{cases} V_o(t) = Ri(t) + L\dfrac{di(t)}{dt} + V_c(t) \\ V_c(t) = \dfrac{1}{c} \oint i(t)\, dt \end{cases} \quad (6)$$

The nonlinear system derivatives of (6) are given by (7):

$$\begin{cases} \dfrac{di(t)}{dt} = -\dfrac{R}{L} i(t) - \dfrac{1}{L} V_c(t) + \dfrac{1}{L} V_o(t) \\ \dfrac{dV_c(t)}{dt} = \dfrac{1}{c} i(t) \end{cases} \quad (7)$$

C. FIRST HARMONIC APPROXIMATION OF STATE VARIABLES

In order to provide the small signal model, we need to calculate $i(t)$ and $V_c(t)$; these states variables are complex values, which can be approximated by (8), where $i_c(t)$, $i_s(t)$ are the real and imaginary parts corresponding to the current $i(t)$ and $V_{cc}(t)$, $V_{cs}(t)$ are the real and imaginary parts corresponding to the voltage $V_c(t)$:

$$\begin{cases} i(t) \approx i_c(t) \cos(\omega_s t) + i_s(t) \sin(\omega_s t) \\ V_c(t) \approx V_{cc}(t) \cos(\omega_s t) + V_{cs}(t) \sin(\omega_s t) \end{cases} \quad (8)$$

The terms $\{i_c,\ i_s,\ V_{cc},\ V_{cs}\}$ are slowly time-varying, thus making it possible to investigate the dynamic behavior of these terms. The derivatives of (8) are found to be:

$$\begin{cases} \dfrac{di(t)}{dt} \approx \left(\dfrac{di_c(t)}{dt} + i_s(t)\omega_s \right) \cos(\omega_s t) \\ \qquad + \left(\dfrac{di_s(t)}{dt} - i_c(t)\omega_s \right) \sin(\omega_s t) \\ \dfrac{dV_c(t)}{dt} \approx \left(\dfrac{dV_{cc}(t)}{dt} + V_{cs}(t)\omega_s \right) \cos(\omega_s t) \\ \qquad + \left(\dfrac{dV_{cs}(t)}{dt} - V_{cc}(t)\omega_s \right) \sin(\omega_s t) \end{cases} \quad (9)$$

D. CONSTRUCTION OF LARGE SIGNAL MODEL

The use of the first harmonic approach gives the opportunity to pass from the exact model to the first harmonic model by replacing the variables $i(t)$ and $V_c(t)$ in (7) by its expressions (5) and (8). In this case, the nonlinear large-signal model of the serial resonance inverter is given by equations (10):

$$\begin{cases} \dfrac{di(t)}{dt} = \begin{pmatrix} -\dfrac{R}{L} \left(i_c \cos(\omega_s t) + i_s \sin(\omega_s t) \right) \\ -\dfrac{1}{L} \left(V_{cc} \cos(\omega_s t) + V_{cs} \sin(\omega_s t) \right) \\ +\dfrac{1}{L} \left(\dfrac{4V}{\pi} \left(\cos(\theta_1) + \cos(\theta_2) \right) \sin(\omega t) \right) \end{pmatrix} \\ \dfrac{dV_c(t)}{dt} = \dfrac{1}{C} \left(i_c \cos(\omega_s t) + i_s \sin(\omega_s t) \right) \end{cases} \quad (10)$$

The simplified form system of equations (10) is given by equations system (11):

$$\begin{cases} \dfrac{di(t)}{dt} = \begin{pmatrix} \left(-\dfrac{R}{L} i_c - \dfrac{1}{L} V_{cc} \right) \cos(\omega_s t) \\ + \begin{pmatrix} -\dfrac{R}{L} i_s - \dfrac{1}{L} V_{cs} \\ + \dfrac{4V}{L\pi} \left(\cos(\theta_1) + \cos(\theta_2) \right) \end{pmatrix} \sin(\omega_s t) \end{pmatrix} \\ \dfrac{dV_c(t)}{dt} = \dfrac{1}{C} i_c \cos(\omega_s t) + \dfrac{1}{C} i_s \sin(\omega_s t) \end{cases} \quad (11)$$

By using the system equations (9) and (11), the following large signal model of the five-level series resonant inverter system can be extracted as follows:

$$\begin{cases} \dfrac{di_c(t)}{dt} = -\dfrac{R}{L} i_c - \dfrac{1}{L} V_{cc} - i_s \omega_s \\ \dfrac{di_s(t)}{dt} = -\dfrac{R}{L} i_s - \dfrac{1}{L} V_{cs} + \dfrac{4V}{L\pi} \begin{pmatrix} \cos(\theta_1) \\ + \cos(\theta_2) \end{pmatrix} + i_c \omega_s \\ \dfrac{dV_{cc}(t)}{dt} = +\dfrac{1}{C} i_c - V_{cs} \omega_s \\ \dfrac{dV_{cs}(t)}{dt} = +\dfrac{1}{C} i_s + V_{cc} \omega_s \end{cases} \quad (12)$$

Equations (12) illustrates the large-signal model; it is a nonlinear system model because it contains the product $(i_s.\ \omega_s)$, $(i_c.\ \omega_s)$, $(V_{cs}.\ \omega_s)$, and $(V_{cc}.\ \omega_s)$, where ω_s, i_s, i_c, V_{cs} and V_{cc} are independent variables. It isn't easy to use the large-signal model to design the control system. After achieving the large-signal model of the system, the nonlinear

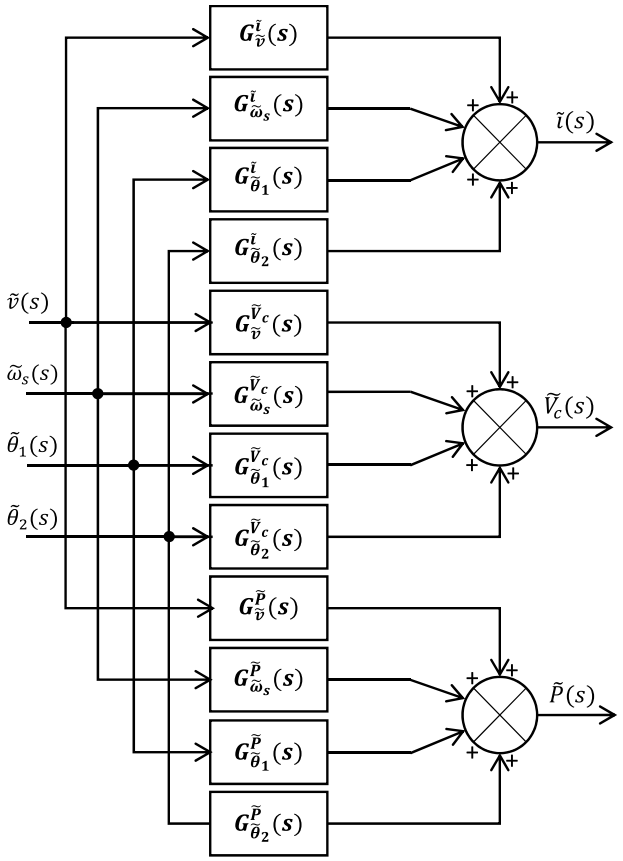

FIGURE 6. Schematic diagram of the inverter in small signal model.

equations can be linearized around the operating point to construct the generalized small-signal transfer function from any desired input (v, θ_1, θ_2, ω_s) to any desired output (i, V_c, p). Fig. 6 shows the mathematical depiction of the proposed circuit in a small-signal model.

For example, we chose to construct the generalized small signal transfer function from the desired input (v, θ_1, θ_2, ω_s) to the output capacitor voltage (V_c). The system inputs $u(t)$, the new state variables $x(t)$, and the output variable $y(t)$ are defined as:

$$\begin{cases} u(t) = \begin{bmatrix} v & \theta_1 & \theta_2 & \omega_s \end{bmatrix}^t \\ x(t) = \begin{bmatrix} i_c & i_s & V_{cc} & V_{cs} \end{bmatrix}^t \\ y(t) = V_c(t) = \sqrt{V_{cc}^2(t) + V_{cs}^2(t)} \end{cases} \tag{13}$$

E. DETERMINATION OF THE EQUILIBRIUM OPERATING POINTS

Setting the derivatives of the large signal model equal to zero, the following equations (14) can be solved to find the equilibrium operating points (I_{c0}, I_{s0}, V_{cc0}, V_{cs0}) of the system.

$$\begin{cases} 0 = -\dfrac{R}{L} I_{c0} - \dfrac{1}{L} V_{cc0} - I_{s0}\omega_{s0} \\ 0 = -\dfrac{R}{L} I_{s0} - \dfrac{1}{L} V_{cs0} + \dfrac{4V}{L\pi} \begin{pmatrix} \cos(\theta_{10}) \\ +\cos(\theta_{20}) \end{pmatrix} + I_{c0}\omega_{s0} \\ 0 = +\dfrac{1}{C} I_{c0} - V_{cs0}\omega_{s0} \\ 0 = +\dfrac{1}{C} I_{s0} + V_{cc0}\omega_{s0} \end{cases} \tag{14}$$

The above equations (14) can be written as matrix forms (15) to found the equilibrium operating points x.

$$\begin{cases} Ax = B \\ x = A^{-1}.B. \end{cases} \tag{15}$$

where:

$$A = \begin{bmatrix} -\dfrac{R}{L} & -\omega_{s0} & -\dfrac{1}{L} & 0 \\ +\omega_{s0} & -\dfrac{R}{L} & 0 & -\dfrac{1}{L} \\ \dfrac{1}{C} & 0 & 0 & -\omega_{s0} \\ 0 & \dfrac{1}{C} & +\omega_{s0} & 0 \end{bmatrix}, \quad x = \begin{bmatrix} I_{c0} \\ I_{s0} \\ V_{cc0} \\ V_{cs0} \end{bmatrix}$$

$$B = \begin{bmatrix} 0 & -\dfrac{4V}{L\pi}\left(\cos(\theta_{10}) + \cos(\theta_{20})\right) & 0 & 0 \end{bmatrix}^t$$

F. DISRUPTION AND LINEARIZATION OF THE LARGE SIGNAL MODEL

Using the Taylor series, the generalized small signal model of the system is derived by perturbation and linearization of large signal model around the operating point (U_0, X_0, Y_0):

$$\begin{cases} x(t) = X_0 + \tilde{x}(t), \quad u(t) = U_0 + \tilde{u}(t), \; y(t) = Y_0 + \tilde{y}(t) \end{cases}$$

where: $\tilde{x}(t) \ll X_0$, $\tilde{u}(t) \ll U_0$, $\tilde{y}(t) \ll Y_0$, and $\tilde{x}(t)$, $\tilde{u}(t)$, $\tilde{y}(t)$: are the small corrections. The perturbation and linearization of the input controls are given as:

$$\begin{cases} \omega_s = \omega_{s0} + \tilde{\omega}_s, \quad \theta_1 = \theta_{10} + \tilde{\theta}_1, \; \theta_2 = \theta_{20} + \tilde{\theta}_2, \; v = V + \tilde{v} \end{cases}$$

The perturbation and linearization of the large signal model (12) of the system is developed to be:

$$\begin{cases} \dot{\tilde{i}}_c = -\dfrac{R}{L}\tilde{i}_c - \dfrac{1}{L} V_{cc} - I_{s0}\tilde{\omega}_s - \tilde{i}_s\omega_{s0} \\ \dot{\tilde{i}}_s = -\dfrac{R}{L}\tilde{i}_s - \dfrac{1}{L}\tilde{V}_{cs} + I_{c0}\tilde{\omega}_s + \tilde{i}_c\omega_{s0} + \dfrac{4}{L\pi}\cos(\theta_{10})\,\tilde{v} \\ \qquad + \dfrac{4}{L\pi}\cos(\theta_{20})\,\tilde{v} - \dfrac{4V}{L\pi}\sin(\theta_{10})\,\tilde{\theta}_1 \\ \qquad - \dfrac{4V}{L\pi}\sin(\theta_{20})\,\tilde{\theta}_2 \\ \dot{\tilde{V}}_{cc} = +\dfrac{1}{C}\tilde{i}_c - V_{cs0}\tilde{\omega}_s - \tilde{V}_{cs}\omega_{s0} \\ \dot{\tilde{V}}_{cs} = +\dfrac{1}{C}\tilde{i}_s + V_{cc0}\tilde{\omega}_s + \tilde{V}_{cc}\omega_{s0} \end{cases} \tag{16}$$

The perturbation and linearization of the output variable of the system is developed to be:

$$\dot{\tilde{y}} = \frac{V_{cc0}}{\sqrt{V_{cc0}^2 + V_{cs0}^2}}\tilde{V}_{cc} + \frac{V_{cs0}}{\sqrt{V_{cc0}^2 + V_{cs0}^2}}\tilde{V}_{cs} \tag{17}$$

G. EXTRACTION OF THE MATRICES {As, Bs, Cs, Ds} OF THE LINEAR MODEL WITH SMALL SIGNALS

In matrix form, the state equations of the small signal model are given as:

$$\begin{cases} \dot{\tilde{x}}(t) = A_s\tilde{x}(t) + B_s\tilde{u}(t) \\ \tilde{y}(t) = C_s\tilde{x}(t) + D_s\tilde{u}(t) \end{cases} \tag{18}$$

where:

$$\begin{cases} \tilde{x}(t) = \begin{bmatrix} \tilde{i}_c & \tilde{i}_s & \tilde{V}_{cc} & \tilde{V}_{cs} \end{bmatrix}^t \\ \tilde{u}(t) = \begin{bmatrix} \tilde{v} & \tilde{\theta}_1 & \tilde{\theta}_2 & \tilde{\omega}_s \end{bmatrix}^t \\ \tilde{y}(t) = \tilde{V}_c \end{cases}$$

The state equations (18) of the small signal model can be described as (19):

$$\begin{cases} \dot{\tilde{x}}(t) = A_s\tilde{x}(t) + B_1\tilde{u}_1(t) + B_2\tilde{u}_2(t) + B_3\tilde{u}_3(t) + B_4\tilde{u}_4(t) \\ \tilde{y}(t) = C_s\tilde{x}(t) \end{cases} \tag{19}$$

where:

$$\tilde{u}_1(t) = \tilde{v}, \quad \tilde{u}_2(t) = \tilde{\theta}_1, \ \tilde{u}_3(t) = \tilde{\theta}_2, \ \tilde{u}_4(t) = \tilde{\omega}_s$$

The transfer functions of input-voltage-to-capacitor-output-voltage, switching-angle-θ_1-to-capacitor-output-voltage, switching-angle-θ_2-to-capacitor-output-voltage, switching-frequency-to-capacitor-output-voltage, respectively, can be written as follows:

$$\begin{cases} G_{\tilde{v}}^{\tilde{V}_c}(s) = \dfrac{\tilde{V}_c(s)}{\tilde{v}(s)} = tf\left(A_s, B_1, C_s, D\right) \\ G_{\tilde{\theta}_1}^{\tilde{V}_c}(s) = \dfrac{\tilde{V}_c(s)}{\tilde{\theta}_1(s)} = tf\left(A_s, B_2, C_s, D\right) \\ G_{\tilde{\theta}_2}^{\tilde{V}_c}(s) = \dfrac{\tilde{V}_c(s)}{\tilde{\theta}_2(s)} = tf\left(A_s, B_3, C_s, D\right) \\ G_{\tilde{\omega}_s}^{\tilde{V}_c}(s) = \dfrac{\tilde{V}_c(s)}{\tilde{\omega}_s(s)} = tf\left(A_s, B_4, C_s, D\right) \end{cases} \tag{20}$$

where:

$$A_s = \begin{bmatrix} -\dfrac{R}{L} & -\omega_{s0} & -\dfrac{1}{L} & 0 \\ +\omega_{s0} & -\dfrac{R}{L} & 0 & -\dfrac{1}{L} \\ \dfrac{1}{C} & 0 & 0 & -\omega_{s0} \\ 0 & \dfrac{1}{C} & +\omega_{s0} & 0 \end{bmatrix},$$

$$B_1 = \begin{bmatrix} 0 & +\dfrac{4}{L\pi}\left(\cos\left(\theta_{10}\right) + \cos\left(\theta_{20}\right)\right) & 0 & 0 \end{bmatrix}^t$$

$$B_2 = \begin{bmatrix} 0 & -\dfrac{4V}{L\pi}\sin\left(\theta_{10}\right) & 0 & 0 \end{bmatrix}^t$$

$$B_3 = \begin{bmatrix} 0 & -\dfrac{4V}{L\pi}\sin\left(\theta_{20}\right) & 0 & 0 \end{bmatrix}^t$$

$$B_4 = [-I_{s0} \quad +I_{c0} \quad -V_{cs0} \quad +V_{cc0}]^t$$

$$C_s = \begin{bmatrix} 0 & 0 & \dfrac{V_{cc0}}{\sqrt{V_{cc0}^2 + V_{cs0}^2}} & \dfrac{V_{cs0}}{\sqrt{V_{cc0}^2 + V_{cs0}^2}} \end{bmatrix}$$

The achieved transfer functions will be divided by appropriate gain approximately equals $\sqrt{2}$ to construct the small signal transfer functions from the inputs to the RMS outputs.

H. VALIDATION OF THE SMALL SIGNAL MODEL

To validate the transfer functions of the developed small-signal model, frequency-domain and time-domain tests are carried out using MATLAB tools, Model Linearizer app under CONTROL SYSTEM APPS and System Identification Toolbox. The first step is validating the small-signal model at resonance frequency f_0 in the frequency-domain, where the frequency responses of the small-signal model are compared with the frequency responses of the Simulink model. The transfer functions of the small-signal model are presented directly using the window command bode(G). The Simulink model is presented based on collected frequency data measurement; the estimation of frequency responses data (frd) of a system is done in MATLAB using the Model Linearizer app. Afterward, the System identification toolbox is used to estimate a parametric presentation of the Simulink model. The second step is confirming the usability of the small-signal model to design a controller in the time-domain, where a PI closed-loop control is used as a testing example.

Fig. 7 shows the Bode diagram frequency responses of the simulation model (Measurement) along with the transfer functions of the small-signal model (Model).

In Bode figures, we presented the frequency responses on all frequency axes for validating the small-signal model, and we did not just use specific frequency points as shown in some previous works, to highlight the most important differences between the linear small-signal model and the switching model build in Simulink. As noted in Fig. 7, the responses of both small-signal and the Simulink model are closely matching. There are certain deviations because only the fundamental component is considered in the small-signal modeling approach. Thus validates the mathematical analysis and the proposed small-signal LTI model.

After testing the small signal model in the frequency domain, the Simulink model and its small signal model are then tested in a closed loop system using the PI controller. Fig. 8 illustrates the common closed-loop system of voltage-mode control using a PI controller. $V_{ref}(t)$, $e(t)$, $V_c(t)$ are the reference, the error and the output voltage, respectively. The PI controller consists of 2 gains, (P) Proportional, and (I) Integral. The controller is auto-tuned using

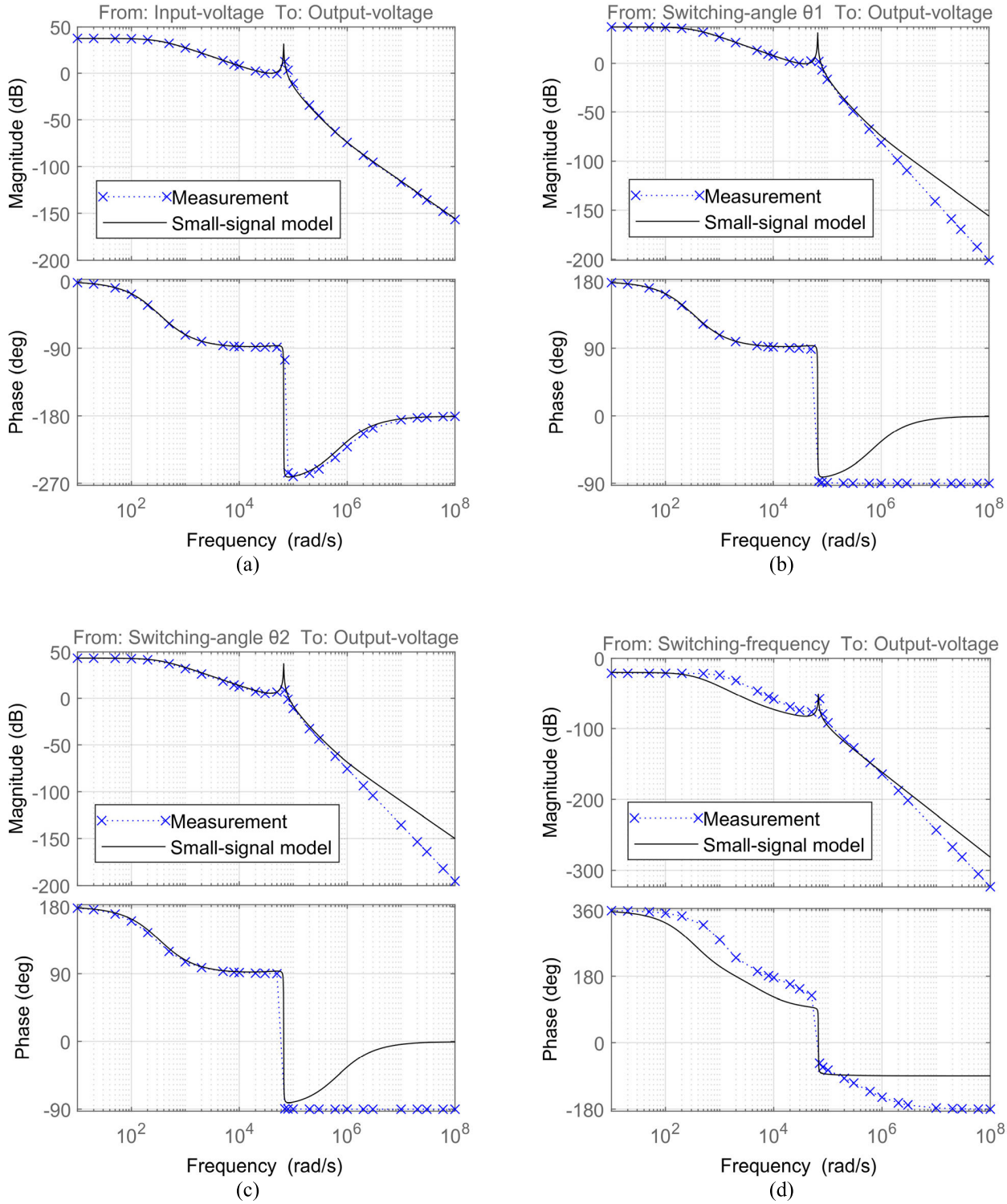

FIGURE 7. Comparisons of Bode plots related to the input control-to-output voltage. (Solid trace): the theoretical small signal model (Model), and (blue cross): Measurement data from simulation model (Measurement). (*a*) : $G_{\tilde{v}}^{\tilde{V}_C}(s)$, (*b*) : $G_{\tilde{\theta}_1}^{\tilde{V}_C}(s)$, (*c*) : $G_{\tilde{\theta}_2}^{\tilde{V}_C}(s)$, (*d*) : $G_{\tilde{\omega}_S}^{\tilde{V}_C}(s)$.

MATLAB tool. Fig. 9 shows the obtained results in time-domain, the small-signal model and the Simulink model responses are in good agreement, thus confirming the usability of the small-signal model for designing controllers.

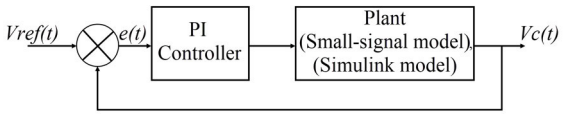

FIGURE 8. A common closed-loop voltage control scheme.

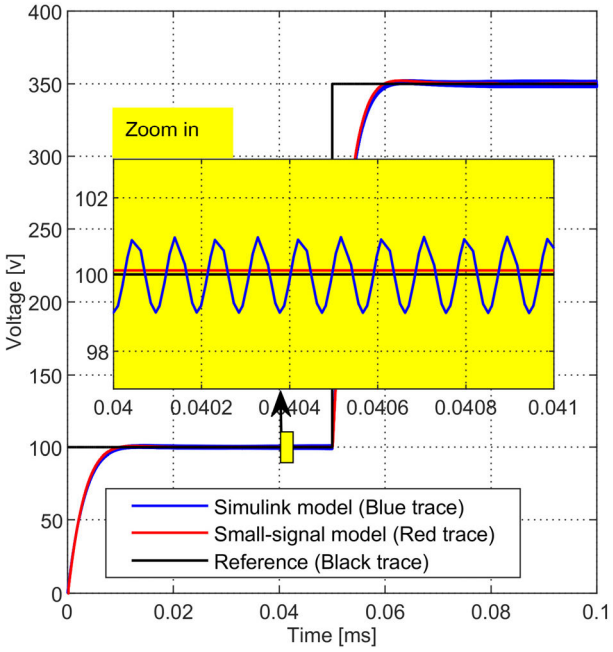

FIGURE 9. Time-domain evaluation showing the small-signal model and Simulink model responses to the same step change.

IV. RESULTS DISCUSSION & INTERPRETATIONS

The proposed circuit of a five-level series resonant inverter is evaluated using simulation and experimental tests. In this section, the results are presented with various switching frequency tests, less than the resonant frequency ($f_s < f_0$), equals the resonant frequency ($f_s = f_0$), and above the resonant frequency ($f_s > f_0$); where the system operating parameters are given in Table 1.

A. SIMULATION RESULTS

Simulation of the five-level series resonant inverter is performed in MATLAB/SimPowerSystems environment. Fig. 10 shows the simulation waveforms of the output inverter voltage $V_{inv}(t)$ and the output capacitor voltage $V_c(t)$ versus the switching frequency (f_s).

Fig. 10(a) displays the waveforms with ($f_s < f_0$) equal to 2 kHz. Two regimes are obviously observed, permanent and transient regimes. The transient regime is imposed by the nonlinearity saturation and hysteresis of electronic components. Inductances and capacitors components are sources of transient voltages in the proposed five-level series resonant inverter. As noticed from the zoom-in from 10 ms to 12 ms, the output inverter voltage $V_{inv}(t)$ and the output capacitor voltage $V_c(t)$ are in the same phase. The output capacitor voltage $V_c(t)$ is sinusoidal, with a maximum value of 13 V, as observed.

TABLE 1. System implementation parameters.

Item.	Ref.	Value
Input Voltage	Vdc	5 Volts
Equivalent Resistance	R	200 Ω
Equivalent Inductance	L	300 mH
Resonant Capacitor	C	3 nF
Resonant frequency	f_0	5.3 kHz
Switching Angle	θ_1	19°
Switching Angle	θ_2	41°
C2000 TMS320F28379D	DSP	200 MHz

Fig. 10(b) displays the waveforms with a switching frequency ($f_s = f_0$) equal to 5.3 kHz. Two regimes are observed, permanent and transient regimes. We can notice that the waveform is quite special, where the wavelength is regularly growing from zero to permanent regime. As seen from the zoom-in from 10 ms to 10.5 ms, the output capacitor voltage $V_c(t)$ is lagging 90 degrees from the output inverter voltage $V_{inv}(t)$ compared with the previous case. The output capacitor voltage $V_c(t)$ is sinusoidal, with a maximum value of 538 V, as observed.

Fig. 10(c) displays the waveforms with switching frequency ($f_s > f_0$) equal to 8 kHz. Two regimes are observed, permanent and transient regimes. As noticed from the zoom-in from 10 ms to 10.33 ms, the output capacitor voltage $V_c(t)$ is lagging 90 degrees from the output inverter voltage $V_{inv}(t)$ compared with the previous case. The output capacitor voltage $V_c(t)$ is sinusoidal, with a maximum value of 8 V, as observed.

B. EXPERIMENTAL RESULTS

A laboratory prototype of the five-level series resonant inverter is realized, as shown in Fig. 11. The control signals are implemented in real-time using an embedded board. GWINSTEK Digital oscilloscope is used to extract the voltage waveforms. Fig. 12(a) displays the gating signals of switches $S_1 \sim S_3$ with a frequency of 5 kHz, and Fig. 12(b) depicts the gating signals of switches $S_4 \sim S_6$.

Fig. 13 illustrates the experimental waveforms of the output inverter voltage $V_{inv}(t)$ and the output capacitor voltage $V_c(t)$ with switching frequency (f_s) equal to 2 kHz. A maximum voltage of 12 V in the capacitor is noted, and RMS voltage equal to 8.23 V is measured.

Fig. 14 illustrates the experimental waveforms of the output inverter voltage $V_{inv}(t)$ and the output capacitor voltage $V_c(t)$ with switching frequency (fs) equal to 5.3 kHz. A maximum voltage of 520 V in the capacitor is noted, and RMS voltage equal to 370.3 V is measured.

Fig. 15 illustrates the experimental waveforms of the output inverter voltage $V_{inv}(t)$ and the output capacitor voltage $V_c(t)$ with switching frequency (f_s) equal to 8 kHz. A maximum voltage of 6 V in the capacitor is noted, and an RMS voltage equal to 4.37 V is measured.

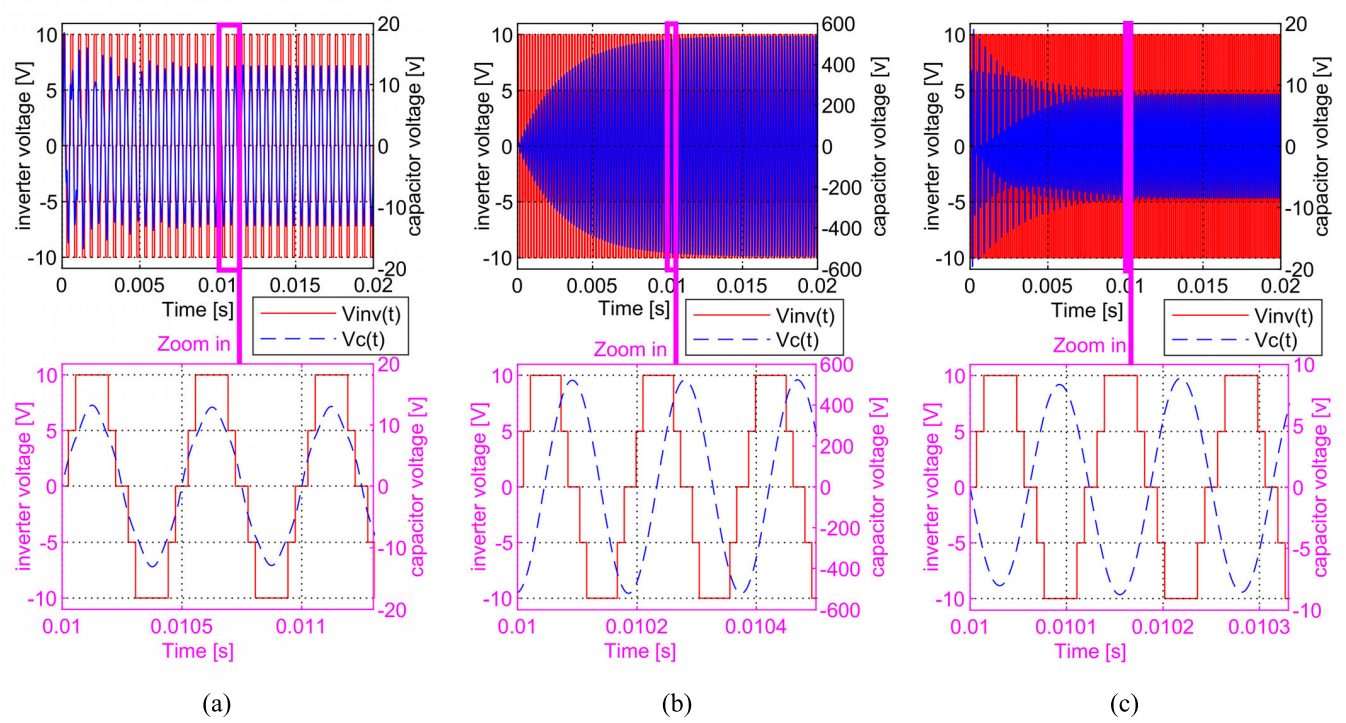

FIGURE 10. Simulation waveforms of output inverter and output capacitor voltages versus the switching frequency (fs). (a): Switching frequency ($f_s < f_0$) equals 2 KHz. (b): Switching frequency ($f_s = f_0$) equals 5.3 KHz. (c): Switching frequency ($f_s > f_0$) equals 8 KHz.

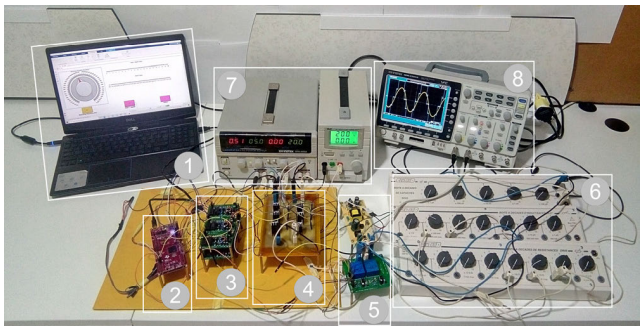

FIGURE 11. A Laboratory prototype equipment's for testing the Five-level series resonant inverter. (1): Pc + Matlab software. (2): C2000 Delfino DSP320F28379D Board. (3): Gate Driver circuits. (4): Inverter (MOSFET switches). (5): Current and voltage sensors. (6): series RLC (Resistor, Inductor, Capacitor) circuit. (7): Power supplies (Vdc). (8): Digital oscilloscope.

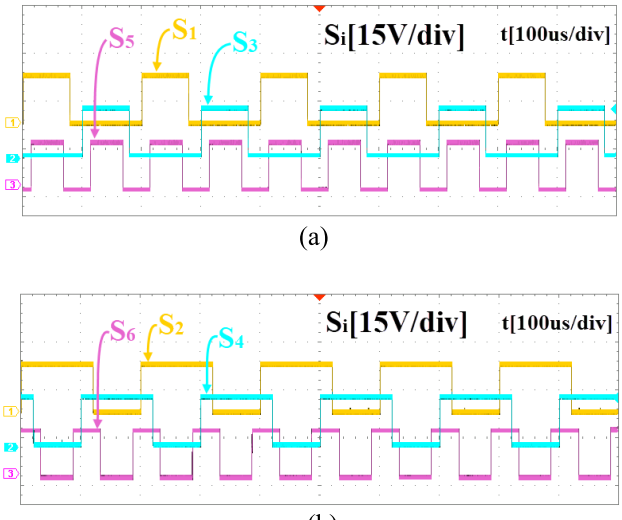

FIGURE 12. The gating signals of $S_1 \sim S_6$ with frequency of 5 KHz.

The experimental results match those observed in the simulation. We can show the similarity that exists between the simulation figures: Figs. 10(a), 10(b), and 10(c) and the experimental figures: Figs. 13, 14, and 15, respectively. Since we have an inductance L and a capacitor C in the series RLC circuit, we distinguish three operation cases depending upon the operating frequency: inductive circuit, capacitive circuit, a resonant circuit; this result is in accord with the conclusions given in [28].

Fig. 16 shows the measured RMS output voltage in capacitor versus variable switching-frequency from 2 kHz to 8 kHz. As noticed from the waveforms, simulation and experimental data are closely matching. At 5.3 kHz, the output capacitor achieves a higher RMS voltage value, approximately equals to 370 V.

The obtained results with the proposed five-level series resonant inverter are in agreement with the findings of previous studies [29] with conventional Full-Bridge inverter; wherein at the resonance frequency: (1) the switching frequency of the inverter approaches the frequency of the series *RLC* circuit;

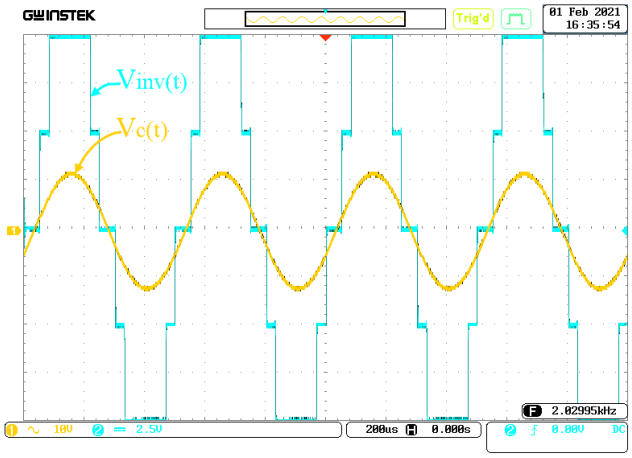

FIGURE 13. Experimental waveforms of output inverter voltage and output capacitor voltage with switching frequency (f_s) equal to 2 kHz.

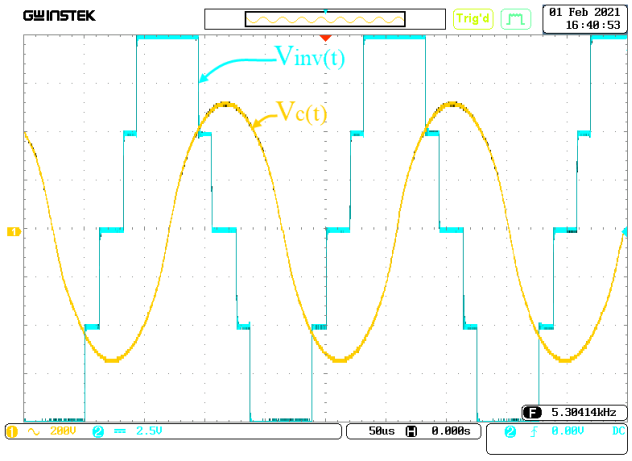

FIGURE 14. Experimental waveforms of output inverter voltage and output capacitor voltage with switching frequency (f_s) equal to 5.3 kHz.

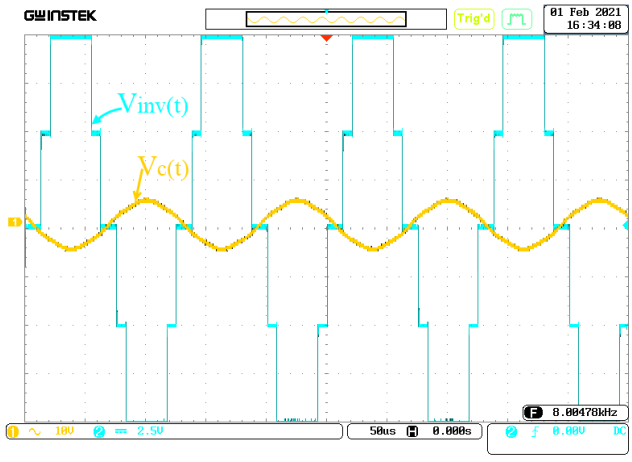

FIGURE 15. Experimental waveforms of output inverter voltage and output capacitor voltage with switching frequency (f_s) equal to 8 kHz.

(2) the inductive reactance equals the capacitive reactance ($X_L = X_C$); thus, the reactance's impact is canceled; and (3) the *RLC* circuit becomes resistive circuit and the output capacitor achieves a higher *RMS* voltage value, and the current becomes maximal.

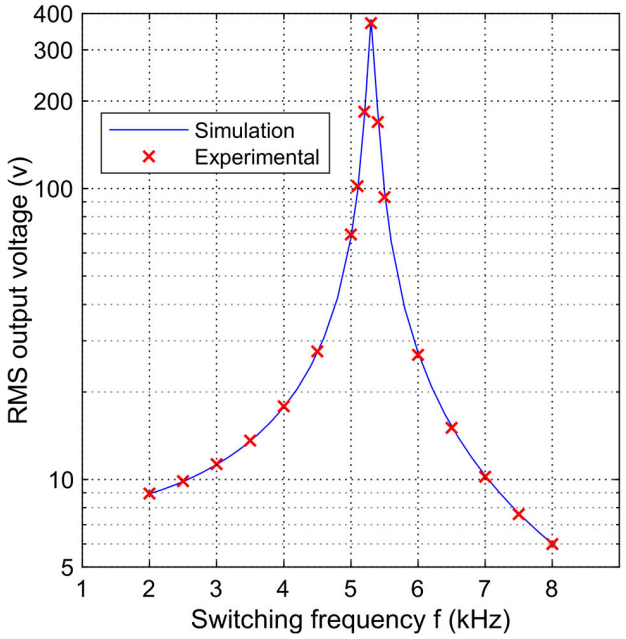

FIGURE 16. Comparison between simulation and experimental results of RMS output capacitor voltage versus switching frequency from 2 kHz to 8 kHz.

V. CONCLUSION

The objective of this study was to develop a small-signal model for a new five-level series resonant inverter. The resonant inverters and the small-signal modeling method are gaining significant popularity in academic research. The proposed circuit has been verified via both simulation and experimental tests with various frequencies. Furthermore, the developed small-signal model has been evaluated in frequency and time domains, also compared with frequency responses and time responses of the validated MATLAB Simulink model. These findings assist our understanding hypothesis that Multilevel-structure can be used in resonant inverters for high-frequency applications and the usability of the small-signal model for designing controllers. The achieved linear time-invariant LTI model of the proposed five-level series resonant inverter will be easily used for control design. The obtained results add to a growing collection of literature on the dynamic modeling of power converters. This work opens new ways for new studies on other power converter topologies.

REFERENCES

[1] F. C. Lee, Q. Li, and A. Nabih, "High frequency resonant converters: An overview on the magnetic design and control methods," *IEEE J. Emerg. Sel. Topics Power Electron.*, vol. 9, no. 1, pp. 11–23, Feb. 2021, doi: 10.1109/JESTPE.2020.3011166.

[2] S.-H. Ryu, D.-G. Woo, M.-K. Kim, and B.-K. Lee, "Analysis and design of modified half-bridge series-resonant inverter with DC-link neutral-point-clamped cell," *IEEE Trans. Power Electron.*, vol. 31, no. 3, pp. 2282–2295, Mar. 2016, doi: 10.1109/TPEL.2015.2431376.

[3] A. Dominguez, L. A. Barragan, J. I. Artigas, A. Otin, I. Urriza, and D. Navarro, "Reduced-order models of series resonant inverters in induction heating applications," *IEEE Trans. Power Electron.*, vol. 32, no. 3, pp. 2300–2311, Mar. 2017, doi: 10.1109/TPEL.2016.2559160.
[4] C. Jiang, K. T. Chau, C. Liu, and C. H. T. Lee, "An overview of resonant circuits for wireless power transfer," *Energies*, vol. 10, no. 7, p. 894, Jun. 2017, doi: 10.3390/en10070894.
[5] X. Tang, Z. Li, and M. Zhang, "A wide-range frequency model for dielectric barrier discharge type ozone generators powered by series resonant inverters," *IEEE Access*, vol. 7, pp. 124309–124314, 2019, doi: 10.1109/ACCESS.2019.2901718.
[6] Y. Wang, O. Lucia, Z. Zhang, S. Gao, Y. Guan, and D. Xu, "A review of high frequency power converters and related technologies," *IEEE Open J. Ind. Electron. Soc.*, vol. 1, pp. 247–260, 2020, doi: 10.1109/OJIES.2020.3023691.
[7] P. R. Bana, K. P. Panda, R. T. Naayagi, P. Siano, and G. Panda, "Recently developed reduced switch multilevel inverter for renewable energy integration and drives application: Topologies, comprehensive analysis and comparative evaluation," *IEEE Access*, vol. 7, pp. 54888–54909, 2019, doi: 10.1109/ACCESS.2019.2913447.
[8] J. S. M. Ali, D. J. Almakhles, S. A. A. Ibrahim, S. Alyami, S. Selvam, and M. S. Bhaskar, "A generalized multilevel inverter topology with reduction of total standing voltage," *IEEE Access*, vol. 8, pp. 168941–168950, 2020, doi: 10.1109/ACCESS.2020.3022040.
[9] A. E. T. Maamar, M. Kermadi, M. Helaimi, R. Taleb, and S. Mekhilef, "An improved single-phase asymmetrical multilevel inverter structure with reduced number of switches and higher power quality," *IEEE Trans. Circuits Syst. II, Exp. Briefs*, vol. 68, no. 6, pp. 2092–2096, Jun. 2021, doi: 10.1109/TCSII.2020.3046186.
[10] B. P. Reddy, M. D. Siddique, A. Iqbal, S. Mekhilef, S. Rahman, and P. K. Maroti, "7L-SCBI topology with minimal semiconductor device count," *IET Power Electron.*, vol. 13, no. 14, pp. 3199–3203, Nov. 2020, doi: 10.1049/iet-pel.2020.0313.
[11] A. Iqbal, M. D. Siddique, B. P. Reddy, and P. K. Maroti, "Quadruple boost multilevel inverter (QB-MLI) topology with reduced switch count," *IEEE Trans. Power Electron.*, vol. 36, no. 7, pp. 7372–7377, Jul. 2021, doi: 10.1109/TPEL.2020.3044628.
[12] A. Iqbal, M. D. Siddique, B. P. Reddy, P. K. Maroti, and R. Alammari, "A new family of step-up hybrid switched-capacitor integrated multilevel inverter topologies with dual input voltage sources," *IEEE Access*, vol. 9, pp. 4398–4410, 2021, doi: 10.1109/ACCESS.2020.3046192.
[13] N. Prabaharan and K. Palanisamy, "A comprehensive review on reduced switch multilevel inverter topologies, modulation techniques and applications," *Renew. Sustain. Energy Rev.*, vol. 76, pp. 1248–1282, Sep. 2017, doi: 10.1016/j.rser.2017.03.121.
[14] X. Yue, X. Wang, and F. Blaabjerg, "Review of small-signal modeling methods including frequency-coupling dynamics of power converters," *IEEE Trans. Power Electron.*, vol. 34, no. 4, pp. 3313–3328, Apr. 2019, doi: 10.1109/TPEL.2018.2848980.
[15] D. Yan, C. Yang, L. Hang, Y. He, P. Luo, L. Shen, and P. Zeng, "Review of general modeling approaches of power converters," *Chin. J. Electr. Eng.*, vol. 7, no. 1, pp. 27–36, Mar. 2021, doi: 10.23919/CJEE.2021.000002.
[16] A. Ayachit and M. K. Kazimierczuk, "Averaged small-signal model of PWM DC-DC converters in CCM including switching power loss," *IEEE Trans. Circuits Syst. II, Exp. Briefs*, vol. 66, no. 2, pp. 262–266, Feb. 2019, doi: 10.1109/TCSII.2018.2848623.
[17] L. Schmitz, D. C. Martins, and R. F. Coelho, "A simple, accurate small-signal model of a coupled-inductor-based DC-DC converter including the leakage inductance effect," *IEEE Trans. Circuits Syst. II, Exp. Briefs*, vol. 68, no. 7, pp. 2533–2537, Jul. 2021, doi: 10.1109/TCSII.2021.3061942.
[18] C. M. Freitas, E. H. Watanabe, and L. F. C. Monteiro, "A linearized small-signal Thévenin-equivalent model of a voltage-controlled modular multilevel converter," *Electr. Power Syst. Res.*, vol. 182, May 2020, Art. no. 106231, doi: 10.1016/j.epsr.2020.106231.
[19] Y. Apertet and H. Ouerdane, "Small-signal model for frequency analysis of thermoelectric systems," *Energy Convers. Manage.*, vol. 149, pp. 564–569, Oct. 2017, doi: 10.1016/j.enconman.2017.07.061.
[20] S. Xu, J. Zhang, Y. Huang, and J. Jatskevich, "Dynamic average-value modeling of three-level T-type grid-connected converter system," *IEEE J. Emerg. Sel. Topics Power Electron.*, vol. 7, no. 4, pp. 2428–2442, Dec. 2019, doi: 10.1109/JESTPE.2019.2894057.
[21] M. D. Benedetto, A. Lidozzi, L. Solero, F. Crescimbini, and P. J. Grbovic, "Small-signal model of the five-level unidirectional T-rectifier," *IEEE Trans. Power Electron.*, vol. 32, no. 7, pp. 5741–5751, Jul. 2017, doi: 10.1109/TPEL.2016.2607839.
[22] K. Mandal, S. Banerjee, and C. Chakraborty, "A new algorithm for small-signal analysis of DC–DC converters," *IEEE Trans. Ind. Informat.*, vol. 10, no. 1, pp. 628–636, Feb. 2014, doi: 10.1109/TII.2013.2277942.
[23] M. Cupelli, A. Riccobono, M. Mirz, M. Ferdowsi, and A. Monti, "Small-signal analysis of cascaded systems," in *Modern Control of DC-Based Power Systems*. New York, NY, USA: Academic, 2018, ch. 2, pp. 15–82, doi: 10.1016/B978-0-12-813220-3.00002-8.
[24] A. Riccobono and A. Turevskiy. (2020). Estimating the frequency response of a power electronics model. MathWorks. Accessed: Apr. 11, 2021. [Online]. Available: https://www.mathworks.com/company/newsletters/articles/estimating-the-frequency-response-of-a-power-electronics-model.html
[25] S. Tian, F. C. Lee, P. Mattavelli, and Y. Yan, "Small-signal analysis and optimal design of constant frequency V^2 control," *IEEE Trans. Power Electron.*, vol. 30, no. 3, pp. 1724–1733, Mar. 2015, doi: 10.1109/TPEL.2014.2320980.
[26] E. X. Yang, F. C. Lee, and M. M. Jovanovic, "Small-signal modeling of series and parallel resonant converters," in *Proc. 7th Annu. Appl. Power Electron. Conf. Expo. (APEC)*, Boston, MA, USA, 1992, pp. 785–792, doi: 10.1109/APEC.1992.228333.
[27] Y.-H. Hsieh, "Accurate small-signal modeling for resonant converters," M.S. thesis, Virginia Polytech. Inst. State Univ., Blacksburg, VA, USA, 2020, pp. 1–25. [Online]. Available: http://hdl.handle.net/10919/100941
[28] M. T. Caccamo, A. Cannuli, and S. Magazù, "Wavelet analysis of near-resonant series RLC circuit with time-dependent forcing frequency," *Eur. J. Phys.*, vol. 39, no. 4, 2018, Art. no. 045702, doi: 10.1088/1361-6404/aaae77.
[29] A. E. T. Maamar, M. Helaimi, and R. Taleb, "Analysis and experimental validation of single phase series resonance inverter," in *Proc. 4th ICEECA*, in Lecture Notes in Electrical Engineering, vol. 682. Singapore: Springer, 2021, pp. 203–216, doi: 10.1007/978-981-15-6403-1_14.

ALLA EDDINE TOUBAL MAAMAR (Graduate Student Member, IEEE) was born in Bouira, Algeria, in April 1993. He received the License degree in electromechanics and the master's degree in electromechanics and control systems from Akli Mohand Oulhadj (AMO) University of Bouira, Bouira, in 2014 and 2016, respectively. He is currently pursuing the Ph.D. degree in electrical control with the Electrical Engineering and Renewable Energy Laboratory (LGEER), Department of Electrical Engineering, Hassiba Benbouali University of Chlef (UHBC), Chlef, Algeria. In 2020, he was a Visiting Researcher with the Power Electronics and Renewable Energy Research Laboratory (PEARL), Department of Electrical Engineering, Universiti Malaya, Kuala Lumpur, Malaysia. His research interests include the design of soft-switching modulation for resonant inverters, analysis and implementation of improved power converters, modeling and advanced control of multilevel inverters, artificial intelligence control, meta-heuristic optimization algorithms, and renewable energy systems.

M'HAMED HELAIMI received the degree in engineering and the Magister degree in electrical engineering from the Hassiba Benbouali University of Chlef (UHBC), Algeria, in 2001 and 2004, respectively, and the Ph.D. degree in electrical engineering from the University of Science and Technology of Oran (USTO), Algeria, in 2014. He joined the Department of Electrical Engineering, Faculty of Technology, UHBC, in 2004. His scientific research interests include optimal tuning methods of controllers, nonlinear system modeling and control, meta-heuristic algorithms, induction heating process, design and implementation of resonant converters, power conversion, and management in micro-grid systems.

RACHID TALEB received the M.S. degree in electrical engineering from the Hassiba Benbouali University of Chlef (UHBC), in 2004, and the Ph.D. degree in electrical engineering from the University of Djillali Liabès, Sidi Bel Abbès, Algeria, in 2011. He is currently a Professor with the Department of Electrical Engineering and the Director of the Laboratoire Génie Electrique et Energies Renouvelables (LGEER) Laboratory, UHBC. His research interests include the design and implementation of multilevel inverters, asymmetrical inverter structures, engineering applications of artificial intelligence, meta-heuristic optimization algorithms, control theory of micro-grid, and renewable energy systems.

MOSTEFA KERMADI (Member, IEEE) received the master's degree in control engineering and the Ph.D. degree in automatic control from the National Polytechnic School (ENP), Algiers, Algeria, in 2012 and 2018, respectively. From December 2016 to July 2018, he was a Visiting Researcher with the Centre of Electrical Energy Systems (CEES), Universiti Teknologi Malaysia (UTM), Malaysia. He is currently a Postdoctoral Research Fellow with the Power Electronics and Renewable Energy Research Laboratory (PEARL), Department of Electrical Engineering, Universiti Malaya, Kuala Lumpur, Malaysia. His scientific research interests include the design and implementation of MPPT controllers, control of power electronic converters, power management in micro-grid, and renewable energy systems.

SAAD MEKHILEF (Senior Member, IEEE) received the B.Eng. degree in electrical engineering from Ferhat Abbas University, Setif, Algeria, in 1995, and the M.Eng.Sc. degree in engineering science and the Ph.D. degree in electrical engineering from the University of Malaya, Kuala Lumpur, Malaysia, in 1998 and 2003, respectively. He is currently a Distinguished Professor with the Faculty of Science, Engineering and Technology, School of Software and Electrical Engineering, Swinburne University of Technology, VIC, Australia, and an Honorary Professor with the Department of Electrical Engineering, Faculty of Engineering, University of Malaya. He has authored or coauthored over 400 academic articles. His research interests include power electronics and renewable energy systems.

ADDY WAHYUDIE (Member, IEEE) received the B.S. degree in electrical engineering (control systems) from Gadjah Mada University, Indonesia, in 2002, the M.Eng. degree in electrical engineering from Chulalongkorn University, Thailand, in 2005, and the D.Eng. degree in electrical engineering from Kyushu University, Japan, in 2010. He was a Lecturer with the Department of Electrical Engineering, Gadjah Mada University, from 2005 to 2011. In 2011, he joined United Arab Emirates University (UAEU), as an Assistant Professor, where he is currently an Associate Professor with the Department of Electrical Engineering. His scientific research interests include control systems theory, such as robust control, model predictive control, intelligent systems control, and its application in electromechanical process, and management of renewable energy.

MUHYADDIN RAWA (Member, IEEE) was born in Makkah, Saudi Arabia, in August 1977. He received the B.Sc. degree in electrical and computer engineering from Umm Al Qura University, in 2000, the M.Sc. degree in electrical and computer engineering, power, and machines from King Abdulaziz University, Saudi Arabia, in 2008, and the Ph.D. degree in electrical and electronic engineering from the University of Nottingham, in 2014. He has over seven years' experiences at Saudi Electricity Company. In 2008, he joined the Department of Electrical and Computer Engineering, King Abdulaziz University, where he is currently an Assistant Professor and the Deputy Director of the Center of Research Excellence in Renewable Energy and Power Systems (CREPS). His scientific research interests include power quality management and control of renewable energy systems.